PNAS RESEARCH ARTICLE | MEDICAL SCIENCES

Optimal deep brain stimulation sites and networks for cervical vs. generalized dystonia

Andreas Horn[a,b,c,1,2], Martin M. Reich[d,1], Siobhan Ewert[a,1], Ningfei Li[a], Bassam Al-Fatly[a], Florian Lange[d], Jonas Roothans[d], Simon Oxenford[a], Isabel Horn[a], Steffen Paschen[e], Joachim Runge[f], Fritz Wodarg[g], Karsten Witt[h], Robert C. Nickl[i], Matthias Wittstock[j], Gerd-Helge Schneider[k], Philipp Mahlknecht[l], Werner Poewe[l], Wilhelm Eisner[m], Ann-Kristin Helmers[n], Cordula Matthies[i], Joachim K. Krauss[f], Günther Deuschl[e], Jens Volkmann[d], and Andrea A. Kühn[a]

Edited by Peter Strick, University of Pittsburgh Brain Institute, Pittsburgh, PA; received August 13, 2021; accepted January 28, 2022

Dystonia is a debilitating disease with few treatment options. One effective option is deep brain stimulation (DBS) to the internal pallidum. While cervical and generalized forms of isolated dystonia have been targeted with a common approach to the posterior third of the nucleus, large-scale investigations regarding optimal stimulation sites and potential network effects have not been carried out. Here, we retrospectively studied clinical results following DBS for cervical and generalized dystonia in a multicenter cohort of 80 patients. We model DBS electrode placement based on pre- and postoperative imaging and introduce an approach to map optimal stimulation sites to anatomical space. Second, we investigate which tracts account for optimal clinical improvements, when modulated. Third, we investigate distributed stimulation effects on a whole-brain functional connectome level. Our results show marked differences of optimal stimulation sites that map to the somatotopic structure of the internal pallidum. While modulation of the striatopallidofugal axis of the basal ganglia accounted for optimal treatment of cervical dystonia, modulation of pallidothalamic bundles did so in generalized dystonia. Finally, we show a common multisynaptic network substrate for both phenotypes in the form of connectivity to the cerebellum and somatomotor cortex. Our results suggest a brief divergence of optimal stimulation networks for cervical vs. generalized dystonia within the pallidothalamic loop that merge again on a thalamo-cortical level and share a common whole-brain network.

deep brain stimulation | dystonia | connectomics | neuromodulation | movement disorders

Significance

We studied deep brain stimulation effects in two types of dystonia and conclude that different specific connections between the pallidum and thalamus are responsible for optimal treatment effects. Since alternative treatment options for dystonia beyond deep brain stimulation are scarce, our results will be crucial to maximize treatment outcome in this population of patients.

Deep brain stimulation (DBS) in patients with treatment-refractory idiopathic dystonia is a well-established therapy with excellent short- and long-term clinical results (1–4). However, in the only controlled trial (1) and its open 5-y follow-up (2), as well as uncontrolled trials with blinded observers (5), around 25% of patients had poor response, which was a primary stimulus for the present work. Moreover, while targeting the internal pallidum (globus pallidus internus, GPi) has been successful, there is still a gap in our understanding of which specific sites within the nucleus lead to network modulation of 1) localized tracts and 2) whole-brain functional networks. Finally, whether targeting could be refined for cervical vs. generalized dystonia has not been investigated in large cohorts, so far.

Here, we revisit a particularly large multicenter cohort (6) with the aim to relate treatment effects to connectional concepts and to investigate potential differences in treatment response of cervical vs. generalized dystonia patients. We do so by introducing a sweetspot-mapping method that is based on electric fields rather than binarized volumes of tissue activated, as well as the recently introduced DBS fiber-filtering (7, 8) and DBS network-mapping (9, 10) approaches.

Hypotheses for this study were established based on two lines of reasoning. The first involves somatotopic organization of the GPi with neurons responding to the orofacial, forelimb, and hindlimb regions of the primary motor cortex located along the ventral-to-dorsal axis in its posterolateral part (11–13). Hence, potentially, ventral stimulation sites could be more specific for responders in cervical dystonia with generalized dystonia optimally responding to a larger or more diffuse stimulation territory. Second, we developed one hypothesis based on the microanatomy of the GPi, which involves that two streams of fibers pass the GPi in largely orthogonal fashion to one another (14, 15). First, there is the extension of the striatopallidofugal system in form of Edinger's comb (connecting striatum and pallidum to the substantia nigra pars reticularis and subthalmic nucleus, STN). Second, there are the pallidothalamic projections (in the form of ansa and fasciculus lenticulares). We aimed to investigate differential effects by leveraging group cohort data of stimulation sites. A more detailed anatomical discussion that led to this hypothesis is given in *SI Appendix* and summarized in Fig. 1.

Author contributions: A.H. designed research; A.H. and S.E. performed research; A.H. and S.O. contributed new reagents/analytic tools; A.H., M.M.R., S.E., N.L., B.A.-F., S.O., and I.H. analyzed data; and A.H., M.M.R., S.E., N.L., B.A.-F., F.L., J. Roothans, S.O., I.H., S.P., J. Runge, F.W., K.W., R.C.N., M.W., G.-H.S., P.M., W.P., W.E., A.-K.H., C.M., J.K.K., G.D., J.V., and A.A.K. wrote the paper.

Competing interest statement: A.H. reports lecture fees fom Medtronic and Boston Scientific outside the submitted work. A.-K.H. reports lecture fees from Medtronic, travel grants from Boston Scientific and Abbott, and personal fees from Aleva, all outside the submitted work. J.K.K. is a consultant to Medtronic and Boston Scientific. A.A.K. reports personal fees from Medtronic, Boston Scientific, and Abbott and Stadapharm, all outside the submitted work.

This article is a PNAS Direct Submission.

[1]A.H., M.M.R., and S.E. contributed equally to this work.

[2]To whom correspondence may be addressed. Email: andreas.horn@charite.de.

This article contains supporting information online at http://www.pnas.org/lookup/suppl/doi:10.1073/pnas.2114985119/-/DCSupplemental.

Published March 31, 2022.

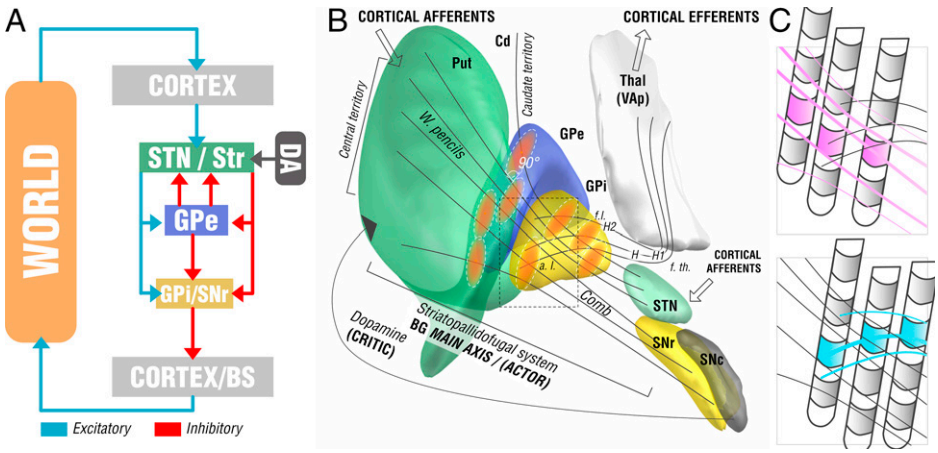

Fig. 1. Functional-anatomical model leading to the core hypothesis for the present study. (*A*) Basal-ganglia model in context of a reinforcement-learning context. The left side shows the main axis of the basal ganglia (actor) with a three-layer model in which both striatum and subthalamic nucleus form entry nodes and GPi and substantia nigra pars reticularis (SNr) serve as output ganglia, feeding information back (via the thalamus) to the cortex and passing it on to brainstem centers (BS). Dopaminergic input serves as one of multiple critics to reinforce successful motor behavior. Adapted from ref. 16. (*B*) Translation of the model to the anatomical domain based on information shown in *SI Appendix*, Fig. S1. The striatopallidofugal system and pallidothalamic fibers serve as the main axis (actor) and receive feedback from dopaminergic centers, especially the substantia nigra pars compacta (SNc). Pallidal receptive fields reside in a 90° angle to the striatopallidofugal fiber system, pallidothalamic output tracts traverse the main axis in equally orthogonal fashion. (*C*) Hypothesis generation for the present study based on anatomical considerations. Two scenarios are possible (shown as cut-out box from *B*). (*Upper*) Active contacts (pink) of top-responding patients are located along the direction of striatopallidonigral fibers. In this case, our results would reveal activation of these fibers to best account for clinical outcome. (*Lower*) Instead, active contacts (cyan) could also be located along pallidothalamic tracts (ansa lenticularis; a.l. and fasciculus lenticularis; f.l.). In this case, our results would reveal activation of these fibers to best account for clinical outcomes.

From this concept, we derived two competing hypotheses that are illustrated in Fig. 1*C*. We registered all DBS electrodes and stimulation volumes to a common space model of the basal ganglia in which the anatomical fiber projections were informed by a recently published and highly accurate pathway atlas of the basal ganglia (17). We hypothesized that three testable scenarios could be present in the data. First, the stimulation volumes of top-responding patients in our sample could be arranged in a way that would not allow any anatomical conclusions (i.e., in a random fashion throughout the cohort). This would favor a null hypothesis according to which our data would not be able to differentiate between the two fiber systems. Alternatively, stimulation volumes from top-responding patients could be arranged in a radial way along the fibers of the striatopallidofugal system, or in an orthogonal way along the pallidothalamic system. In case one of those scenarios would hold true, our data could associate one of the two fiber systems with optimal clinical outcomes.

Here, we aimed to address this question using the DBS fiber-filtering method to isolate tracts that are predominantly associated with top-responding patients in cervical vs. generalized dystonia. The method was introduced in rudimentary form in 2019 (7) and has been subsequently refined (8, 18). We complemented the approach by a sweetspot-mapping algorithm that directly works on electric fields instead of binarized stimulation volumes. Here, the aim was to map optimal stimulation sites to somatotopic regions within the GPi (*Methods*). Finally, to complement results with a "broad-lens view" that would include polysynaptic networks, we applied the DBS network-mapping approach to identify whole-brain functional networks that accounted for optimal treatment response (9).

Methods

Patient Cohorts and Imaging. Eighty DBS patients from five different centers were retrospectively included in this study after meticulous inspection of imaging quality (25 patients were excluded due to poor imaging quality after visual inspection). Six of 22 tested patients with generalized dystonia were DYT1^{+}; 1 was DYT25^{+}. Patients with cervical dystonia and 12 patients with generalized dystonia did not undergo genetic testing. All patients underwent DBS surgery for either cervical ($n = 46$) or generalized ($n = 34$) dystonia and received two quadripolar DBS electrodes (either model 3389 or 3387; Medtronic). The surgical procedure was similar in all centers, and has been described previously (19). The neurostimulation parameters were programmed according to best clinical practice by the local DBS neurologist, based on clinical response testing. All video sequences were rated retrospectively by the same movement disorder neurologist (M.M.R.), using either the Toronto Western Spasmodic Torticollis Rating Scale (TWSTRS) in subjects with cervical dystonia or the Burke–Fahn–Marsden Dystonia Rating Scale (BFMDRS) in patients with generalized or segmental dystonia (in the following referred to as generalized dystonia). Results were normalized by calculating the percentage change of the TWSTRS and the BFMDRS. In subjects with cervical dystonia, the TWSTRS motor score improvement without using the duration factor (item Ib) was assigned to both hemispheres equally; this modified motor score was chosen because the total TWSTRS motor score is too strongly weighted by the duration factor with respect to the improvement of dystonic postures (19). In subjects with generalized or segmental dystonia, the global improvement in BFMDRS was associated with the stimulation of both hemispheres. All patients received preoperative MRI and neuropsychological testing to exclude structural or severe psychiatric comorbidities. After surgery, patients received postoperative MRI or CT imaging to confirm electrode placement. All patients signed an informed consent form for the recording and storage of all personal data (e.g., video sequences) and the study was conducted in accordance with the Declaration of Helsinki and approved by the Institutional Review Board of the University Hospital of Würzburg (registry number 150/15).

DBS Electrode Localizations and E-Field Modeling. DBS electrodes were localized using the advanced processing pipeline (20) in Lead-DBS [https://www.lead-dbs.org/ (21); RRID:SCR_002915]. In short, postoperative CT or MRI were linearly coregistered to preoperative MRI using advanced normalization tools [https://stnava.github.io/ANTs/ (22)]. Coregistrations were inspected and refined if needed. A brain-shift correction step was applied as implemented in Lead-DBS. All preoperative volumes were used to estimate a precise multispectral normalization to ICBM 2009b NLIN asymmetric (MNI) space (23) applying the advanced normalization tools SyN Diffeomorphic Mapping (24) using the preset "effective: low variance default + subcortical refinement" in Lead-DBS. This approach was top-performer to segment the GPi with precision comparable to manual expert segmentations in a recent comparative study (25), which was

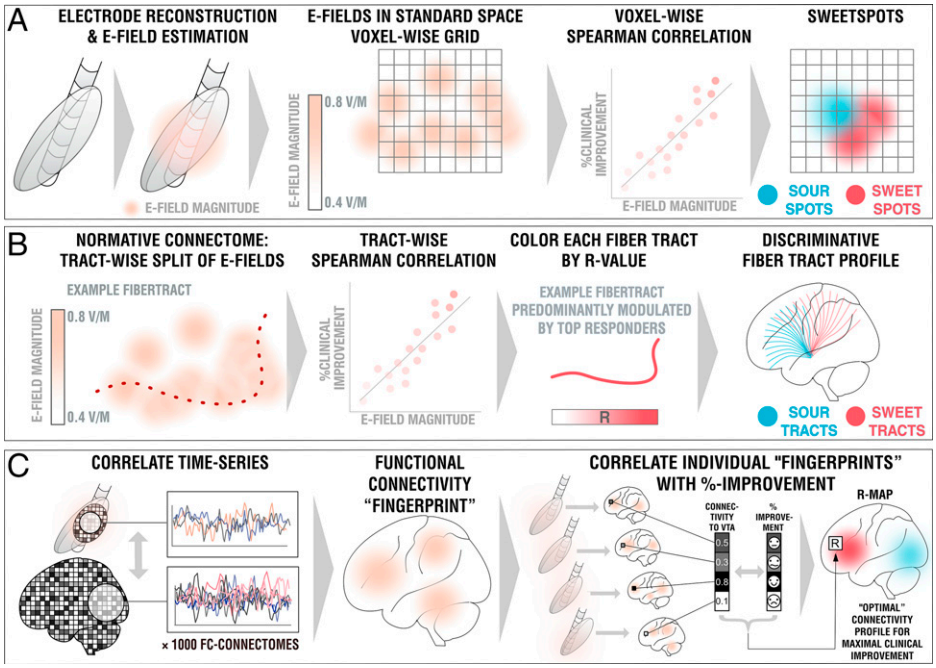

Fig. 2. Overview of the three methods applied. (*A*) DBS sweetspot mapping. Based on DBS electrode localizations carried out with Lead-DBS, E-fields were estimated using a finite element approach based on the long-term stimulation parameters applied in each patient. E-fields were then warped into MNI space. For each voxel, the E-field vector magnitudes and clinical improvements were rank-correlated, leading to a map with positive and negative associations (sweet and sour spots). (*B*) DBS fiber filtering. Again, E-fields were pooled in standard space and the group was set into relationship with all of 26,800 tracts forming a predefined set of normative pathways (17). Sum E-field magnitudes along each tract were aggregated for each patient and again rank-correlated with clinical improvements, attributing positive vs. negative weights to each tract (sweet and sour tracts). (*C*) DBS network mapping. Seeding blood-oxygen level-dependent signals from each E-field in a database of 1,000 healthy brains led to functional connectivity maps that were averaged to form a functional connectivity "fingerprint" for each patient. Voxels in these were correlated with clinical improvements to create an R-map model of optimal network connectivity.

further replicated by a different group (26). Normalization warp-fields were further manually adapted using the respective module in Lead-DBS (27), as well as a reiteration of the approach, termed "WarpDrive" (28). DBS contacts were automatically prereconstructed using the phantom-validated and fully-automated PaCER method (29) or the TRAC/CORE approach (21) and manually refined if needed. Atlas segmentations in this report are defined by the DISTAL atlas (30). Group visualizations were performed using the Lead group toolbox (31).

Electric fields (E-fields) were estimated in native space based on the long-term DBS settings applied using an adaptation of the SimBio/FieldTrip pipeline (32), as implemented in Lead-DBS (20). Briefly, using the finite element method, the static formulation of the Laplace equation was solved on a discretized domain represented by a tetrahedral four-compartment mesh (composed of gray and white matter, metal, and insulating electrode parts). Electric fields were transformed to MNI space using the same refined normalization warpfields described above. Since no lateralized effects were expected (6), for all subsequent analyses, E-fields were nonlinearly flipped to the other hemisphere in order to overlay $2 \times 80 = 160$ E-fields across the whole cohort. Fourteen of the 80 patients had bipolar stimulation settings on at least one hemisphere. Electric fields for bipolar settings were calculated in the same fashion.

Modeling Considerations. Estimated after Pakkenberg and Gundersen (33), each cubic millimeter of the cortex is filled with ~170,000 neurons, each with an average number of ~10,000 inputs and outputs. According to numbers aggregated by Bergman (34), the GPi is less densely populated, with only ~1,000 neurons per cubic millimeter. For axonal numbers, following Zalesky and Fornito (35), each fiber bundle in a standard neuroimaging analysis represents 10^3 to 10^5 tightly packed axons. Many DBS studies aimed at modeling discretized and realistic axonal cable models in the past (36–38). However, given these sheer numbers of axons involved, here we chose to assume probabilistic axonal populations in each brain voxel and represented by each fiber tract, instead of modeling representative single axons. Such populations will have more diffuse firing properties that could encode numeric variables, rather than following an all-or-nothing firing property that would be assumed for single axons (39). While single axons fire in an all-or-nothing fashion, activations of larger axonal populations within a voxel may be better represented by a probabilistic fashion, which is dependent on the applied voltage (40–42). In other words, on a population level, the "degree" of activation will be stronger under higher voltages applied or when closer to the electrodes. Crucially, there is a large amount of uncertainty about the exact relationship between voltage and axonal firing that needs patient-specific calibration, even when applying more realistic biophysical models (37). Since this relationship is unclear, we applied Spearman's rank correlations in our sweetspot and fiber-filtering models. We believe that this simple model could have a crucial advantage, since it would show maximal values ($R \rightarrow 1.0$) for any type of function that is monotonically increasing. In other words, the concept could be robust toward the exact relationship (be it linear, cubic, or logistic) between amplitude and modulation.

DBS Sweetspot Mapping.

Model in Fig. 2A. Using E-fields calculated in each patient, and the aforementioned considerations in mind, a unique approach to define optimal stimulation sites was applied (Fig. 2*A*), which was inspired by the DBS network-mapping approach introduced earlier (also, see below and ref. 9). E-fields represent the first derivative of the estimated voltage applied to voxels in space and their vector magnitudes are thus stronger in the proximity of active electrode contacts, with a rapid decay over distance. For each voxel covered by the group of E-fields across the cohort in MNI space, E-field vector magnitudes across patients were Spearman rank-correlated with clinical improvements. Since not all voxels were covered by the same amount of E-fields, the area of interest was restricted to voxels that were at least covered by 30% of E-fields with a vector magnitude above 150 V/m, which is around a typical value that has been assumed to activate axons (43). The resulting sweetspot maps would peak at voxels in which stronger E-fields were associated with better treatment responses. The map would have negative values for voxels with the opposite relationship.

Estimates. Mutliplying each voxel of a single E-field with the resulting sweetspot map and calculating the sum across voxels led to estimates of how a specific E-field would perform (i.e., estimates of clinical improvements following DBS). If the E-field peaked at similar locations as the sweetspot map, a high

estimate would result. If it would peak at a valley of the map, low or even negative estimates would result.

DBS Fiber Filtering.

Model in Fig. 2B. For a finite set of 28,600 subcortical fibertracts represented within the Basal Ganglia Pathway Atlas (17) and each E-field in each patient, a value of probabilistic impact on the tract was calculated by summing the E-field magnitude vectors along the tract. This led to a matrix of 28,600 × 160 dimension, each entry denoting the sum "impact" of each E-field on each tract. Again, the exact relationship between E-field magnitude and activations of axonal populations is dependent on multiple of factors unknown in the individual patient (axonal shape, diameters, myelinization, degrees of arborization of both dendritic and axonal terminals, numbers of nodes of Ranvier, conductivity of axonal, interstitial vs. myelin components, degree of microstructural anisotropy, heterogeneity and dispersivity of tissue conductivity, specific properties of the encapsulation layer, capacitive properties, and so forth). Hence, again, Spearman's rank correlations were chosen that would account for any type of monotonically increasing function. This led to a model of 28,600 correlation coefficients (one for each tract), showing positive values for tract populations maximally "impacted" by electrodes in top responding patients and negative values for the ones preferentially modulated in poor responding patients. While a second, similarly detailed pathway atlas, which includes comb fibers and accurate depictions of ansa and fasciculus lenticulares in part traversing through the pallidum, is not available to the best of our knowledge, we repeated the analysis based on a confirmatory dataset of subcortical bundles reconstructed based on diffusion tractography (44).

Estimates. In a similar fashion, single E-fields were probed based on the estimated tract model. If their "peaks" resided on positively weighted tracts and their "valleys" on negatively (or less positively) weighted tracts, they received a high-score estimate. Again, the exact (linear or nonlinear) relationship remains elusive; so, we applied Spearman's rank correlations a third time.

DBS Network Mapping.

Model in Fig. 2C. In a last approach, we calculated whole-brain functional connectivity estimates seeding from E-fields based on a library of resting-state functional MRI (rs-fMRI) scans acquired in 1,000 healthy participants (45, 46), following the approach of Horn et al. (9). This method allowed to investigate the functional connectivity profile of a specific DBS electrode within the average human brain, and the resulting maps have been termed connectivity fingerprints, previously (10). In analogy to the sweetspot model, voxel-wise correlations between Fisher *z*-scored connectivity strengths and clinical improvements were calculated, which led to R-map models of optimal connectivity. Here, Pearson's correlations were applied since underlying values are normal-distributed and linear relationships could be assumed (in comparison, E-fields used above are composed of highly skewed distributions). As for sweetspot- and tract-filtering models, one DBS network-mapping model was calculated for cervical and generalized dystonia cases, separately. However, given the more broad-lens view these models impose, one additional model was calculated on the entire cohort. Finally, following the approach of Li et al. (10), an agreement map was calculated between cervical and generalized models, which retained only voxels that had the same sign in both models (and multiplicated their absolute values). The latter was performed to identify potential common denominators in network effects across cervical and general dystonia types.

Estimates. Spatial similarities between single connectivity fingerprints and R-map models were calculated using voxel-wise spatial correlations. This led to positive high correlation values for cases in which fingerprints graphically matched the (optimal) connectivity profile represented by the R-map model, and lower or even negative values for other cases.

Results

Electrodes of all patients were placed with their active contacts within or close to the GPi (Fig. 3). Clinical results of this retrospective cohort are described in more detail, elsewhere (6). Briefly, our DBS cohort included 80 patients operated at five different DBS centers (38 female, mean age 48.3 ± 16.0 y), 46 with cervical and 34 with generalized dystonia (Table 1).

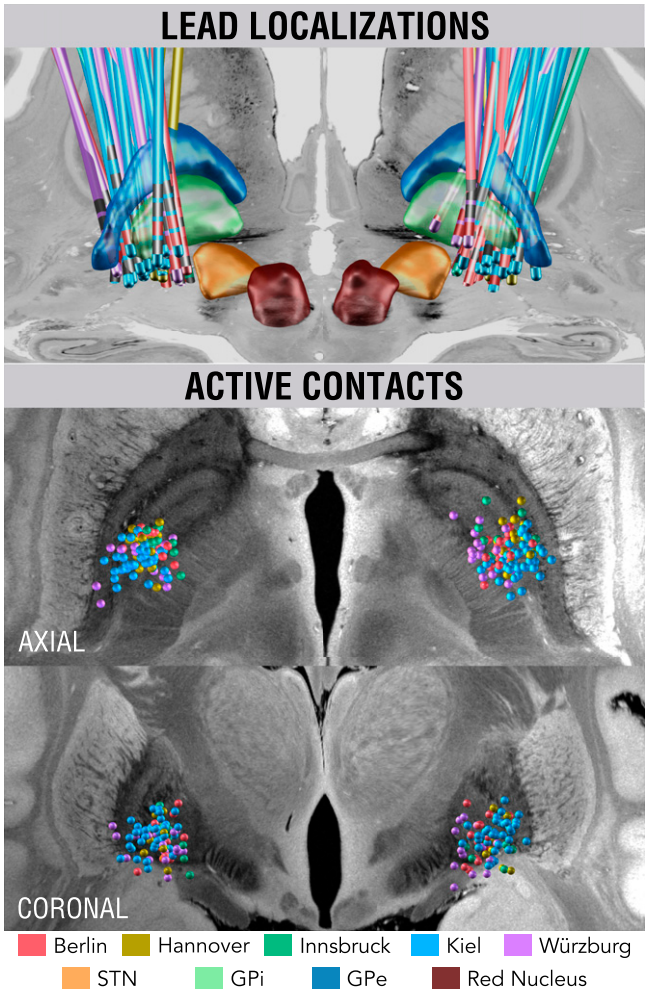

Fig. 3. Reconstructions of DBS electrode placement of the five cohorts color-coded by center (*Top*). Active DBS contacts of the group shown in synopsis with an ultrahigh-resolution template of the human brain (27).

On a local level (DBS sweetspot mapping), voxels in the posterior ventromedial GPi were associated with optimal improvements of the cervical cohort, whereas voxels equally medial but at a slightly more anterior and dorsal subregion of the GPi were most associated with improvements in the cohort with generalized dystonia. The cervical sweetspot map peaked at ±20.4, −12.4, $z = -5.2$ mm (MNI coordinates; with a Spearman's rank correlation coefficient of $R = 0.58$), which was located precisely at the medial pallidal border and a mere 2.6-mm apart from the maximal sweetspot coordinate reported by Reich et al. (6) (±19.4, −10.1, −5.9 mm) (6). This is important given their spot was calculated with a completely different methodological pipeline. Similarly, the spot precisely matched the finding by Mahlknecht et al. (47) in cervical dystonia. The generalized sweetspot map peaked at ±21.1, −9.1, $z = -0.14$ mm ($R = 0.67$): that is, more dorsal and anterior, and about 6-mm apart from both the cervical spot and the optimal coordinate reported by Reich et al. (6).

When visualized in the context of the GPi, cervical sweetspot regions localized to the cervical somatotopic motor region of the pallidum, as described by Nambu (12), which map to the ventral border of the pallidum. Following probabilistic conversion to AC/PC coordinates (48), the cervical sweetspot mapped to 19.57 ± 1.42-mm lateral to, 0.01 ± 0.90-mm anterior to, and 1.87 ± 0.72-mm below the midcommissural point. The generalized sweetspot mapped to 20.22 ± 1.53-mm lateral to,

Table 1. Patient demographics

DBS center	Mean age	*n* cervical (female)	*n* generalized (female)	*n* total (female)	%-Clinical Improvements (cervical)	%-Clinical Improvements (generalized)	%-Clinical Improvements (combined)
Berlin	51.4 ± 16.7	4 (2)	6 (1)	10 (3)	28.6 ± 50.8	51.3 ± 28.8	42.2 ± 38.2
Hannover	47.9 ± 17.8	7 (3)	2 (1)	9 (4)	48.7 ± 42.6	36.1 ± 44.1	44.5 ± 40.7
Innsbruck	46.3 ± 15.2	5 (3)	2 (0)	7 (3)	49.4 ± 22.3	73.9 ± 22.9	58.8 ± 24.8
Kiel	47.0 ± 15.3	22 (13)	19 (7)	41 (20)	66.0 ± 27.1	73.9 ± 22.9	69.9 ± 25.2
Würzburg	50.8 ± 18.6	8 (4)	5 (4)	13 (8)	48.0 ± 31.9	87.7 ± 11.3	66.3 ± 31.4
Total	48.3 ± 16.0	46 (25)	34 (13)	80 (38)	55.2 ± 33.0	69.9 ± 27.3	62.0 ± 31.2

This table shows basic phenotypic parameters (age, case numbers, and clinical improvements across each center's cohorts).

2.83 ± 1.03-mm anterior to, and 2.95-mm above the mid-commissural point. Generalized sweetspot regions were more outstretched, potentially incorporating a larger somatotopic fraction of the motor pallidum (see last panel of Fig. 5, which shows a summary of sweetspot results). The exact peaks of this spot resided in two sites, dorso-anterior and ventral to the cervical peak, which could potentially associate with the trajectory of the ansa lenticularis, which has been described to course ventrally to the pallidum (6, 49). Beyond this ventral site, in synopsis with a homuncular projection adapted from Nambu (12), the largest peak resided within the hand and trunk region of the pallidum (Fig. 4).

On a tract level, from all 28,600 fiber bundles included within the Basal Ganglia Pathway Atlas (17), the clinical outcomes in the cervical cohort correlated most with 1) pallidosubthalamic fibers in the posterior (i.e., motor) part of Edinger's comb system and 2) corticospinal fibers of passage connecting to the head and neck region of the sensorimotor cortex (Fig. 5). Indeed, this finding is in agreement with the medial position of sweetspots identified in the present study and the one by Reich et al. (6). We must emphasize that methodological constraints hinder us from concluding with certainty whether in the actual brain of patients these tracts would indeed map to: 1) fibers of passage, 2) corticopallidal tracts (which are sparse but present), 3) peri-pallidal projections to cortex as described by Parent et al. (51), or 4) corticospinal/corticopontine projections. Crucially, in the cervical cohort, fasciculus lenticularis and a more anterior part of Edinger's comb (still within its motor domain) were negatively associated with optimal clinical outcomes. In the cohort with generalized dystonia, tracts most associated with optimal outcomes were the pallidothalamic tracts (i.e., fasciculus and ansa lenticulares), as well as some of the more anteriorly situated comb fibers. Instead, some even more medially located fibers of passage within the internal capsule were negatively associated with optimal outcomes. Fig. 5*B* summarizes these results.

When lowering the visualization threshold to allow for a more broad-lens view on involved networks, tracts associated with optimal outcomes in cervical dystonia involved the cortical connections to the head/neck region of the somatomotor cortex, while regions to the full somatotopic spectrum were associated with positive outcomes in the generalized dystonia cohort (Fig. 5*A*). This finding was largely replicated when using a second pathway atlas that was based on diffusion tractography (44) (*SI Appendix*, Fig. S2). The two models explained ∼23% ($R = 0.48$; $P < 0.001$) and ∼28% ($R = 0.53$; $P < 10^{-16}$) of variance within the whole sample but we must emphasize that this analysis was circular and can merely express the degree-of-fit between data and model. To test whether the resulting correlation would solely be based on circularity of the model, we calculated random permutations (×5,000 iterations) and recalculated the same model and correlations after permuting improvement values across cohorts. Results from runs with permuted improvement values defined the null-distribution to which the unpermuted run was compared. The sum of the two R values ($0.48 + 0.53 = 1.01$) was significantly larger in the unpermuted vs. the permuted cases ($P = 0.005$) (Fig. 5*C*).

To further extend these insights, we applied the DBS network-mapping approach on estimates of whole-brain functional connectivity as informed by a normative connectome obtained from 1,000 healthy brains. While the structural connectivity estimates from the Basal Ganglia Pathway Atlas (17) could investigate, which specific localized connections accounted for clinical outcomes, this additional analysis asked the same question for distributed whole-brain networks that could include indirect, polysynaptic connections, as well. Again, functional connectivity to different sets of regions were associated with optimal outcomes for cervical vs. generalized cohorts, which are summarized in *SI Appendix*, Table S1 and shown in Fig. 6. Most saliently, generalized dystonia was associated with stronger anticorrelations to whole sensory cortices (where in contrast cervical dystonia specifically to the homuncular head/neck regions). Improvements in cervical dystonia were associated with positive connections to the supplementary motor area and posterior cingulate cortex, while in generalized dystonia, the same was true for the ventral anterior cingulate cortex and precuneus. When pooling across all patients irrespective of dystonia type ("combined" panel in Fig. 6), anticorrelations to the somatosensory cortex and positive connections to the cerebellum, supplementary motor area, and cingulate cortex were favored. Finally, we calculated an agreement map to visualize regions that positively or negatively correlated in both subcohorts alone, which revealed positive connections to cerebellum and midbrain regions, as well as anticorrelations to somatomotor temporal and inferior frontal cortices.

Discussion

Three main conclusions can be drawn from our study. First, we show evidence that optimal stimulation sites for cervical and generalized dystonia map to different target regions, tracts, and whole-brain networks. Specifically, our results suggest that optimal stimulation sites within the pallidum map to somatotopic pallidal regions: that is, the ventral head/neck motor zone of the GPi for maximal benefit in cervical dystonia and a more diffuse mapping to the motor part of the pallidum for generalized dystonia. Second, we show results that suggest specific connections could play a key role in mediating treatment benefit in cervical vs. generalized dystonia. While modulating pallidothalamic tracts accounted for

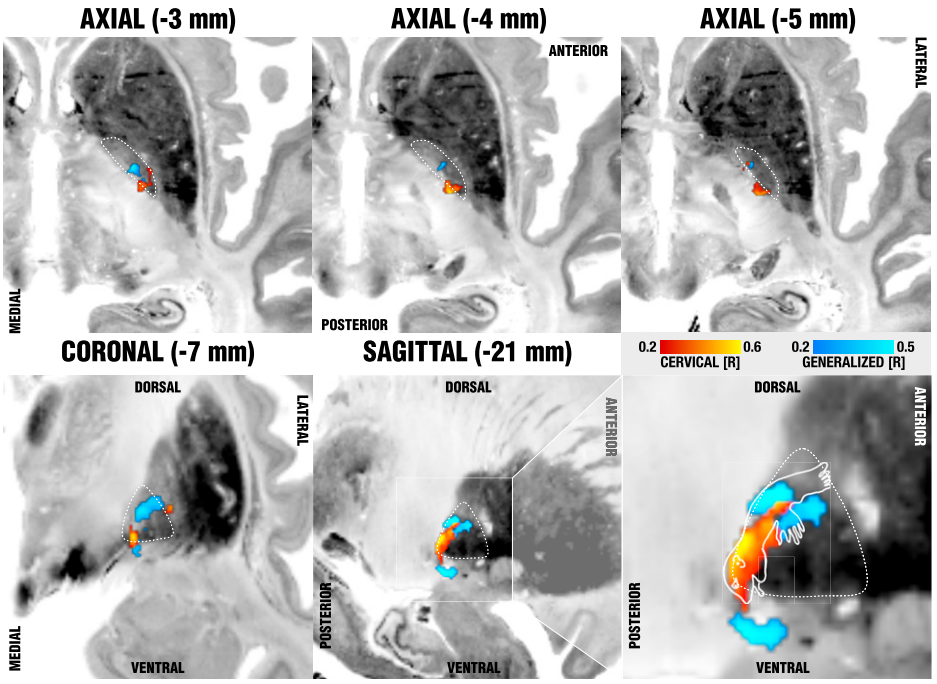

Fig. 4. Sweetspot mapping of cervical (red) vs. generalized (blue) subcohorts matches somatotopic organization of the GPi as defined by Nambu (12). Voxels are color-coded by the degree of correlation between percent improvements of either TWSTRS (cervical, hot colors) or BFMDRS (generalized, cool colors) and shown on multiple axial (*Upper*) and coronal/sagittal (*Lower*) slides on top of the BigBrain template (50). The last panel (*Lower Right*) shows the homuncular representation of the pallidum following reports by Nambu (12), which stated that neurons responding to the orofacial, forelimb, and hindlimb regions of motor cortex are located along the ventral-to-dorsal axis in the GPi.

optimal improvements in generalized dystonia, specific corticofugal tracts connecting to head/neck regions of the somatomotor cortex, as well as a specific subpart of pallidosubthalamic connections, accounted for effects observed in cervical dystonia. Third, we investigated which whole-brain functional networks would account for optimal treatment success. Analysis again suggested the involvement of differential networks with a common substrate that, inter alia, involved positive connections to the cerebellum and negative connections to the somatomotor cortex.

As the most salient finding, our report sheds light on a potential segregation between optimal stimulation sites for cervical vs. generalized dystonia at the pallidal level. Namely, stimulation of the striatopallidofugal bundle was associated with optimal improvement in cervical dystonia, and pallidothalamic tracts were with optimal improvements in generalized dystonia. While these systems are segregated, they have a clear common path back to the thalamus and cortex and both coincide with cerebellar input at the thalamic level. We believe these insights could be highly relevant and suitable to form novel hypotheses but must emphasize potential limitations of the model and techniques (see below) and believe that further confirmation will be mandatory going forward.

Localized Stimulation Model. Several optimal stimulation sites within the pallidal region have been suggested for dystonia in the past. Some have concluded that optimal stimulation sites would be localized in the intersection between the internal and external pallidum (52, 53). A large study, which had analyzed the same sample, concluded on a more ventral position, which resided in part ventral and medial to (outside of) the pallidum (6). Here, the focus had been to generate a predictive modeling framework that was able to account for ∼50% of variance in clinical outcomes in out-of-sample data (i.e., patients not seen by the model).

The match between somatotopic pallidal regions and optimal results in cervical and generalized dystonia could be one possible reason for seemingly heterogeneous results in past studies. Regions that did account for optimal outcomes in cervical dystonia indeed precisely mapped to the ventral motor part of the pallidum, as suggested by somatotopic mapping data conducted in primates (12). On the other hand, optimal stimulation sites for generalized dystonia spanned across larger parts of the motor pallidum, including the interface between the internal and external pallidum [e.g., as reported by Starr et al. (52)], as well as the portion ventrally to the pallidum reported by Reich et al. (6). Indeed, as reported in Reich et al. (6), a cluster resided ventromedially to the GPi. Hence, somatotopy of the disease could play a major role especially on the dorsoventral axis of the GPi. Needless to say, others have suggested this before. For example, Vayssiere et al. (11) concluded that inside the posterolateroventral subvolume of the GPi on the right side, three statistically different locations of electrode contacts were determined to be primary DBS treatment sites for particular body parts in cases of dystonia, a notion that our findings confirm. The sweetspot mapping approach we propose here may have the advantage of not being limited to spherical and binary tissue activation models and, at least in theory, would be able to shape sweetspots of any geometrical form. In combination with the large sample size of our study, the somatotopic results we show could be seen as a useful addition. The regions will be made available under an open license within Lead-DBS software, which could facilitate confirmatory (or directly contradictory) follow-up studies on additional samples.

Tract-Level Stimulation Model. To expand on the second notion (anatomical considerations), as mentioned in the Introduction, the pallidum contains two massive and orthogonal systems of fibers. On one hand, the striatopallidofugal system traverses the pallidum radially (connecting cortex → striatum → external →

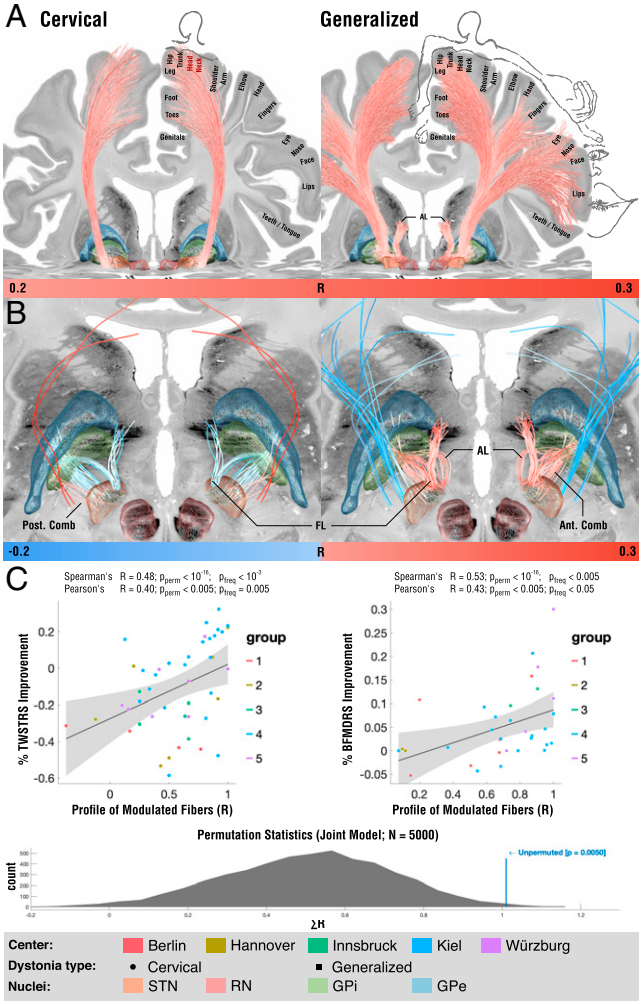

Fig. 5. Tracts associated with optimal outcome for patients with cervical (*Left*) and generalized (*Right*) dystonia. (*A*) On a broader scale (slightly lower threshold), modulation of corticofugal tracts from the somatomotor head and neck region weas associated with optimal outcomes in cervical dystonia, while tracts from the whole somatotopical domain were associated with generalized dystonia. (*B*) On a localized level (slightly higher threshold), in cervical dystonia, striatopallidofugal tracts of the posterior comb system were associated with optimal outcomes. In contrast, fibers from the fasciculus lenticularis were negatively associated. In generalized dystonia, both pallidothalamic bundles (ansa and fasciculus lenticularis) were associated with optimal outcomes, as was a more anterior portion of the comb system. (*C*) Across the cervical and generalized cohorts, the degree of how fittingly the identified networks were modulated by each patient's E-field correlated with clinical improvements. While these correlation analyses are of circular nature, a permutation statistic (*Bottom*) showed superior model fits for unpermuted vs. permuted improvement values. AL: ansa lenticularis, FL: fasciculus lenticularis.

GPi and → STN/substantia nigra with many interconnections among regions), which we termed the "main axis of the basal ganglia" in the Introduction. On the other hand, the pallidum is traversed orthogonally to the main axis by the pallidothalamic projections, which are thought to form a continuum and include fasciculus and ansa lenticularis (15, 54). This leads us to the second stage of our model, which aimed at modeling exactly these differential fiber systems.

To briefly summarize tract-based findings again: modulating posterior pallidosubthalamic/nigral fibers (main axis) accounted for optimal outcomes in cervical dystonia, while modulating pallidothalamic fibers for generalized dystonia, both with the common projection back to the thalamus. While the former would be thought to map more strongly onto the indirect pathway (with the STN) and use the nigra as output structure, the latter would primarily implement the GPi as output structure. We especially deem the latter finding crucial since, as mentioned, the pallidothalamic bundles traverse the whole pallidum and could integrate information from all pallidal regions. Hence, speculatively, disruption at this system could lead to more generalized symptoms not limited to specific body parts. In turn, widely parallel fibers radially projecting from the pallidum through the internal capsule (i.e., extending the parallel striatopallidofugal fibers) could be affected in a more symptom and somatotopy-specific fashion. We must emphasize that this notion is and remains speculative, and could only be confirmed and deliberately tested in animal models and axon-specific modulation strategies (e.g., using optogenetics). A more intuitive second finding was that those fibers of passage projecting from head/cervical vs. generalized somatotopic regions of the somatomotor cortex differentially accounted for variance in outcomes in the respective dystonia type. Alterations in the somatomotor cortex, specifically in plasticity of the sensory cortices, have been proposed to play a crucial pathophysiological role in dystonia (55–60).

Recently, Corp et al. (61) applied lesion network mapping to investigate shared networks of stroke lesions that led to cervical dystonia, which again attributed a specific role to the somatosensory cortex. Hence, our findings that successful treatment of cervical dystonia, at least by the somatotopic domain, maps to connections of specifically the head/cervical zones and generalized dystonia to the full somatotopic domain of the somatomotor cortex could form crucial additional support for pathophysiological involvement of the somatomotor cortex. In this context, however, it is crucial to emphasize that direct projections from cortex to pallidum are not classically described in the gross-anatomical literature and, hence, may at least not exist in large numbers. While reports about such direct connections [also between an aforementioned peripallidal site around the GPi and cortex (51)] have been described using robust methods that are not prone to false-positive connections (62) (for an overview, also see figure 25 in ref. 63), the largest proportion of cortical input to the pallidum is transmitted via the massive projection of the striatopallidofugal bundle (49). Hence, the direct cortical connections our analysis revealed could be truly pathophysiologically relevant. Alternatively, they could express the specific region of the pallidum that would likely receive corticostriatal input from the same cortical regions, given the orderly fashioned organization of the whole cortico-basal ganglia thalamic loops (30, 64, 65).

On a whole-brain level that could involve polysynaptic connections, a region of longstanding interest for the pathophysiology of dystonia is the cerebellum (66). This leads us to the final stage of our model, which involved the broad-lens view of whole-brain functional networks.

Network-Level Stimulation Model. On a whole-brain level, the aforementioned study by Corp et al. (61) revealed that lesions that led to cervical dystonia would be positively connected to the cerebellum and negatively to the sensory cortex. Crucially, among the few regions with connections that did account for symptom improvement following DBS regardless of dystonia type were exactly these two regions with the same signs as described by Corp et al. (61) (agreement map in Fig. 6). Specifically, the positive connections to wider parts of the cerebellum were positively associated with optimal outcomes in both cervical and generalized dystonia. Functional involvement of the cerebellum could be mechanistically implemented by malfunctions of the sodium-

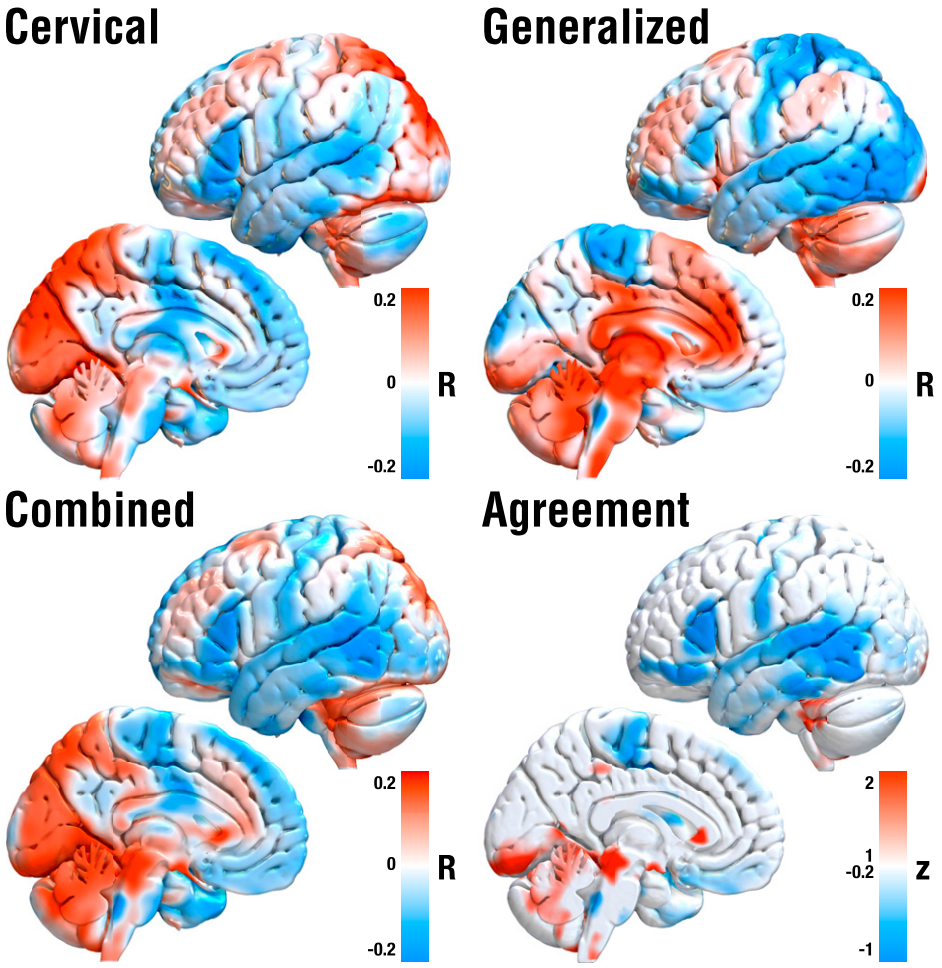

Fig. 6. DBS network-mapping results based on normative rs-fMRI data. Red regions show connections positively correlated with clinical improvements, blue regions the opposite. Crucially, optimal networks in cervical vs. generalized dystonia differed substantially but both included positive connections to cerebellum and midbrain regions and negative to somatomotor, temporal and inferior frontal cortices (as revealed by both the combined and agreement maps).

potassium pump in cerebellar Purkinje neurons (67), with ouabain blocks of the pump leading to dystonic symptoms in mouse models (68). Clinical reports involve the disappearance of dystonic symptoms after cerebellectomy (69) and substantial antidystonic effects after DBS to the cerebellum, even after failed bilateral pallidotomy and intrathecal baclofen therapy (70). Hence, while dystonia has traditionally been regarded as a basal ganglia disorder, enough evidence has accumulated that its pathophysiology involves cortico-ponto-cerebello-thalamo-cortical loops as well. In the human motor thalamus, cerebellar and basal ganglia afferents are thought to map to different thalamic nuclei, which may be identified by axonal tracing studies in animals (51) or by staining for distribution patterns of glutamic acid decarboxylase isoform 65 (71).

Furthermore, while basal ganglia input to the thalamus maps to matrix cells, which diffusely project to apical cortical layers, cerebellar thalamic input predominantly maps to core cells that focally project to basal dendrites of layer five cortical neurons (65, 72). This has led to the notion that the cerebellar function in movement embodies a system to automatize certain types of movements after motor learning (65, 73). By doing so, thalamocortical connections integrate cerebellar and basal ganglia input to orchestrate cortical activity and plasticity (65) [due to transition to burst-mode firing of cortical neurons in case of simultaneous activation of apical and basal dendrites (74)]. Our results show supporting evidence for the involvement of exactly these pallidothalamic projections for the case of generalized dystonia (and multisynaptic involvement of the cerebellum). In the case of cervical dystonia, results suggest an indirect connection via the subthalamic nucleus but similar polysynaptic involvement of the cerebellum. Alternatively, the pallidosubthalamic fibers could represent pallidonigral projections, which are impossible to differentiate by means of neuroimaging given their intertwined course within Edinger's comb system. In the latter case, nigrothalamic projections and multisynaptic cerebellar involvement would constitute an analogous finding to the one described in generalized dystonia.

Above and beyond the cerebellum and somatomotor cortex, network results included positive associations with midbrain regions (tectum and tegmentum), which could be interpreted as a continuum with cerebellar results (since the cerebellar peduncle traverses through the midbrain). In line with this, pontomesencephalic lesions to the tectum and tegmentum have been associated with the occurrence of secondary dystonia (75). In animal studies, nigro-tectal pathway lesioning led to reduced inhibition of the superior colliculus, which led to symptoms of cervical dystonia (76). Furthermore, our results included negative associations with inferior frontal and temporal cortices. Metabolic changes have been reported in both frontal and temporal association areas in patients with focal and generalized dystonia (77–79). Specifically, reorganization of the inferior frontal gyrus was associated with compensatory mechanisms to inhibitory control in focal dystonia (80). Using combined local field potential and magnetoencephalographic

recordings in dystonia patients, our own group provided electrophysiological evidence about communication between the pallidum and temporal cortices in the θ-band, which were contrasted by connections to somatomotor cortices (β-band) and the cerebellum (α-band) (81). The exact causal contributions or compensatory nature of these regions in dystonia remain elusive. Using our method (fMRI), we can merely provide further evidence that the aforementioned regions seem to play a role in mediating treatment for both cervical and generalized dystonia.

Limitations. Multiple limitations on various levels apply to the present study. First and foremost, the retrospective nature of the study should be emphasized, as well as the analysis of the same multicenter cohort in the study by Reich et al. (6). Still, the sample constitutes the largest cohort studied by means of DBS imaging to date, and we believe that studying it with different methods and approaches will be beneficial for treating dystonia going forward. Along the same lines, the sample involves heterogeneous imaging datasets as well as clinical records that were acquired during clinical routine. This adds to the inherent imprecision of DBS electrode localizations that can be substantial and largely depend on imaging quality (38); however, it could also be seen as a strength since variability in the data may lead to more robust findings not overfit to data from a specific surgeon/center. Similarly, our results are limited to determine optimal stimulation sites based on the anatomical landscape covered by DBS electrodes (i.e., will at best represent most effective locations given the assumptions already made by the neurosurgeons). The multicenter nature of the study (total of seven neurosurgeons) may again provide benefit here. We applied a modern imaging pipeline that has been specifically developed to localize DBS electrodes, including multispectral normalizations (30), manual warpfield refinements (27), and brain-shift correction (20), as well as phantom-validated electrode localizations (29). Automatic segmentations of the GPi derived with the pipeline rivaled the precision of manual expert segmentations in a study that investigated multiple nonlinear registration approaches for the subcortex (25) and a second study that confirmed results (26).

Furthermore, manual refinement of registrations was applied in a labor-intensive patient-by-patient process to ensure precise fit between the atlas model of the pallidum and the patient-specific MRI data (27). Still, a certain degree of imprecision is inherent to this process and must be acknowledged. One general limitation of studies that map DBS effects to sweetspots and networks for symptoms that are not asymmetric (such as limb tremor that can be quantified for the two sides of the body separately) is that two data points (i.e., two electrodes and stimulation sites) account for a single value (symptom improvements). Hence, it always remains ambiguous which data point (or whether both) account for the symptom improvement. Multiple strategies have been proposed to account for this (6, 82, 83), but no single strategy is clearly superior to the other. As in the study by Reich et al. (6), in this study, we chose to assume symmetric effects of DBS, and hence mirrored stimulation sites between the two hemispheres of the brain.

Third, on the tract level, the accuracy and anatomical validity of the basal ganglia pathway model is an important condition to interpret our results. Here, slight misrepresentations of the anatomical detail of implemented tracts could have large impact on results. For example, the intrapallidal course of the pallidothalamic output fibers would likely play a role in segregating results for cervical and generalized dystonia. While the pathway model has been curated by world-renowned basal ganglia anatomists (17) and constitutes the best anatomical model our field currently has, it has been indirectly defined in humans [and, for instance, was largely informed by macaque tracer studies (84)] and, as any normative atlas resource, does not account for individual variability. Alternatively, normative diffusion MRI (dMRI)-based connectomes could be used but have shown poor resolution of the small subcortical tracts identified here (e.g., ansa lenticularis, comb fibers, and so forth) in direct comparison studies (38). Identification of these bundles is hence limited to supervised reconstruction using high-resolution (or group-level) dMRI data and placement of manual waypoints (44, 85). Here, we could in part confirm our results using such a manually curated pathway atlas that was constructed from dMRI data acquired in 1,000 healthy brains. However, some details (such as y-shaped axon collateral configurations in hyperdirect pathways, comb fibers or ansa/fasciculus lenticulares traversing through the pallidum) were not available in this dataset and are currently unique to the holographic basal ganglia atlas created by Petersen et al. (17). Given the poor resolution of dMRI scans in a clinical setting (typically not below 1.5 mm for isotropic voxels), this limitation applies to individual connectomes (calculated from patient-specific dMRI data) as well, and may apply even more so to cohorts prone to movement artifacts (such as dystonia) (86). Finally, the technique developed and applied here (DBS fiber filtering) is by design limited to normative tractograms, since the exact same bundle needs to be tested in all patients. Hence, interpretation of especially the tract-level results of the present study should be seen as a function of anatomical validity of the tract atlas.

Fourth, the biophysical model electrical effects on the tissue was modeled in a comparably simplified manner, where more advanced concepts have been introduced, in the past (36, 37, 87). While more advanced biophysical modeling options have now been introduced as open-source and interfaced within the Lead-DBS software applied here (88), as mentioned in *Methods*, in the present study the choice of a simple model was indeed deliberate. Modeling an electric field is a simpler engineering task, which is often followed by modeling biology (i.e., the response of neurons and axons). A downside of the latter approach is the necessity to impose a large set of assumptions. Instead, herein we did apply concepts that would not be susceptible to the exact relationship between stimulation amplitude and the degree of neuromodulation on the axonal populations surrounding the electrodes. Instead, the model (concretely implemented by means of mass-univariate rank-correlations) would yield maximal weights for any type of monotonically increasing relationship between the two.

Conclusions

We report evidence that cervical vs. generalized dystonia responds optimally to neuromodulation of a specific set of striatopallidofugal and pallidothalamic connections and that treatment effects involve indirect connections with the cerebellum and somatomotor cortex. Specific optimal stimulation sites in the pallidum map to somatotopic representations of the nucleus, with the optimal stimulation site for cervical dystonia mapping to its cervical functional zone. We construct a model that involves local, tract- and network-based components that

explain significant amounts of clinical variance following DBS to the pallidum.

Data Availability. The DBS MRI datasets generated and analyzed during the present study are not publicly available due to data privacy regulations of patient data, but are available from the corresponding author on reasonable request (A.H.). The study consists of a reanalysis of data from a prospective trial (6) with cases dating back to 2004 at multiple centers; hence, patient consent for data sharing could not be obtained. All code used to analyze the dataset is available within Lead-DBS/-Connectome software at GitHub (https://github.com/netstim/leaddbs).

ACKNOWLEDGMENTS. The study was supported by a Dystonia Medical Research Foundation & Cure Dystonia Now grant on Brain Networks in Dystonia (to A.H. and A.A.K.); the German Research Foundation (Deutsche Forschungsgemeinschaft) Emmy Noether Stipend 410169619 (to A.H.) and 424778381-TRR 295 (to A.H., M.M.R., G.-H.S., C.M., J.V., and A.A.K.); Deutsches Zentrum für Luft- und Raumfahrt (DynaSti grant within the EU Joint Programme Neurodegenerative Disease Research) (to A.H.); the Foundation for Obsessive Compulsive Disorder Research (A.H.); and Interdisziplinäres Zentrum für Klinische Forschung (IZKF) of the University Hospital Wuerzburg (Grant number Z-2/64) (for M.M.R.).

Author affiliations: [a]Movement Disorder and Neuromodulation Unit, Department of Neurology, Charité–Universitätsmedizin Berlin, corporate member of Freie Universität Berlin and Humboldt-Universität zu Berlin, 10117 Berlin, Germany; [b]Center for Brain Circuit Therapeutics, Department of Neurology, Brigham & Women's Hospital, Harvard Medical School, Boston, MA 02115; [c]Massachusetts General Hospital Neurosurgery, Center for Neurotechnology and Neurorecovery, Massachusetts General Hospital, Harvard Medical School, Boston, MA 02114; [d]Department of Neurology, Julius-Maximilians University Würzburg, 97070 Würzburg, Germany; [e]Department of Neurology, University Kiel, 24118 Kiel, Germany; [f]Department of Neurosurgery, Medical School Hannover, 30625 Hannover, Germany; [g]Department of Radiology, University Kiel, 24118 Kiel, Germany; [h]Department of Neurology, University Oldenburg, 26129 Oldenburg, Germany; [i]Department of Neurosurgery, Julius-Maximilians University Würzburg, 97070 Würzburg, Germany; [j]Department of Neurology, University Rostock, 18051 Rostock, Germany; [k]Department of Neurosurgery, Charité–Universitätsmedizin Berlin, corporate member of Freie Universität Berlin and Humboldt-Universität zu Berlin, 10117 Berlin, Germany; [l]Department of Neurology, Innsbruck Medical University, 6020 Innsbruck, Austria; [m]Department of Neurosurgery, Innsbruck Medical University, 6020 Innsbruck, Austria; and [n]Department of Neurosurgery, University Kiel, 24118 Kiel, Germany

1. A. Kupsch *et al.*; Deep-Brain Stimulation for Dystonia Study Group, Pallidal deep-brain stimulation in primary generalized or segmental dystonia. *N. Engl. J. Med.* **355**, 1978–1990 (2006).
2. J. Volkmann *et al.*; DBS study group for dystonia, Pallidal deep brain stimulation in patients with primary generalised or segmental dystonia: 5-year follow-up of a randomised trial. *Lancet Neurol.* **11**, 1029–1038 (2012).
3. E. Moro *et al.*, Efficacy of pallidal stimulation in isolated dystonia: A systematic review and meta-analysis. *Eur. J. Neurol.* **24**, 552–560 (2017).
4. A. M. Lozano *et al.*, Deep brain stimulation: Current challenges and future directions. *Nat. Rev. Neurol.* **15**, 148–160 (2019).
5. M. Vidailhet, P. Pollak, Deep brain stimulation for dystonia: Make the lame walk. *Ann. Neurol.* **57**, 613–614 (2005).
6. M. M. Reich, A. Horn, F. Lange *et al.*, Probabilistic mapping of antidystonic effect of pallidal neurostimulation: Multicentre imaging study. *Brain* **142**, 1386–1398 (2019).
7. J. C. Baldermann *et al.*, Connectivity profile predictive of effective deep brain stimulation in obsessive-compulsive disorder. *Biol. Psychiatry* **85**, 735–743 (2019).
8. N. Li *et al.*, A unified connectomic target for deep brain stimulation in obsessive-compulsive disorder. *Nat. Commun.* **11**, 3364 (2020).
9. A. Horn *et al.*, Connectivity predicts deep brain stimulation outcome in Parkinson disease. *Ann. Neurol.* **82**, 67–78 (2017).
10. N. Li *et al.*, A unified functional network target for deep brain stimulation in obsessive-compulsive disorder. *Biol. Psychiatry* **90**, 701–713 (2021).
11. N. Vayssiere *et al.*, Deep brain stimulation for dystonia confirming a somatotopic organization in the globus pallidus internus. *J. Neurosurg.* **101**, 181–188 (2004).
12. A. Nambu, Somatotopic organization of the primate basal ganglia. *Front. Neuroanat.* **5**, 26 (2011).
13. K. L. K. Au, J. K. Wong, T. Tsuboi *et al.*, Globus pallidus internus (GPi) deep brain stimulation for Parkinson's disease: Expert review and commentary. *Neurol. Ther.* **10**, 7–30 (2021).
14. G. Percheron, J. Yelnik, C. François, A Golgi analysis of the primate globus pallidus. III. Spatial organization of the striato-pallidal complex. *J. Comp. Neurol.* **227**, 214–227 (1984).
15. M. Parent, A. Parent, The pallidofugal motor fiber system in primates. *Parkinsonism Relat. Disord.* **10**, 203–211 (2004).
16. M. Deffains *et al.*, Subthalamic, not striatal, activity correlates with basal ganglia downstream activity in normal and Parkinsonian monkeys. *eLife* **5**, 4854 (2016).
17. M. V. Petersen, J. Mlakar, S. N. Haber *et al.*, Holographic reconstruction of axonal pathways in the human brain. *Neuron* **104**, 1056–1064.e3 (2019).
18. F. Irmen *et al.*, Left prefrontal impact links subthalamic stimulation with depressive symptoms. *Ann. Neurol.* **87**, 962–975 (2020).
19. J. Volkmann *et al.*; DBS Study Group for Dystonia, Pallidal neurostimulation in patients with medication-refractory cervical dystonia: A randomised, sham-controlled trial. *Lancet Neurol.* **13**, 875–884 (2014).
20. A. Horn *et al.*, Lead-DBS v2: Towards a comprehensive pipeline for deep brain stimulation imaging. *Neuroimage* **184**, 293–316 (2019).
21. A. Horn, A. A. Kühn, Lead-DBS: A toolbox for deep brain stimulation electrode localizations and visualizations. *Neuroimage* **107**, 127–135 (2015).
22. B. B. Avants *et al.*, A reproducible evaluation of ANTs similarity metric performance in brain image registration. *Neuroimage* **54**, 2033–2044 (2011).
23. V. S. Fonov, A. C. Evans, R. C. McKinstry, C. R. Almli, D. L. Collins, Unbiased nonlinear average age-appropriate brain templates from birth to adulthood. *Neuroimage* **47**, S102 (2009).
24. B. B. Avants, C. L. Epstein, M. Grossman, J. C. Gee, Symmetric diffeomorphic image registration with cross-correlation: Evaluating automated labeling of elderly and neurodegenerative brain. *Med. Image Anal.* **12**, 26–41 (2008).
25. S. Ewert, A. Horn, F. Finkel, N. Li, A. A. Kühn, T. M. Herrington, Optimization and comparative evaluation of nonlinear deformation algorithms for atlas-based segmentation of DBS target nuclei. *NeuroImage* **184**, 586–598 (2019).
26. D. Vogel, A. Shah, J. Coste, J. J. Lemaire, K. Wårdell, S. Hemm, Anatomical brain structures normalization for deep brain stimulation in movement disorders. *NeuroImage Clin.* **27**, 102271 (2020).
27. B. L. Edlow *et al.*, 7 Tesla MRI of the ex vivo human brain at 100 micron resolution. *Sci. Data* **6**, 244 (2019).
28. S. Oxenford *et al.*, Lead-OR: A multimodal platform for deep brain stimulation surgery. medRxiv[Preprint] (2020). https://www.medrxiv.org/content/10.1101/2021.08.09.21261792v1 (Accessed 1 January 2022).
29. A. Husch, M. V Petersen, P. Gemmar, J. Goncalves, F. Hertel, PaCER–A fully automated method for electrode trajectory and contact reconstruction in deep brain stimulation. *Neuroimage Clin.* **17**, 80–89 (2017).
30. S. Ewert *et al.*, Toward defining deep brain stimulation targets in MNI space: A subcortical atlas based on multimodal MRI, histology and structural connectivity. *Neuroimage* **170**, 271–282 (2018).
31. S. Treu, B. Strange, S. Oxenford *et al.*, Deep brain stimulation: Imaging on a group level. *Neuroimage* **219**, 117018 (2020).
32. J. Vorwerk, L. Magyari, J. Ludewig, R. Oostenveld, C. H. Wolters, The fieldtrip-simbio pipeline for finite element EEG forward computations in MATLAB: Validation and application. First International Conference on Basic and Clinical Multimodal Imaging BaCI, Geneva, Switzerland; August 9, 2013.
33. B. Pakkenberg, H. J. Gundersen, Neocortical neuron number in humans: Effect of sex and age. *J. Comp. Neurol.* **384**, 312–320 (1997).
34. H. Bergman, *The Hidden Life of the Basal Ganglia* (MIT Press, 2021).
35. A. Zalesky, A. Fornito, A DTI-derived measure of cortico-cortical connectivity. *IEEE Trans. Med. Imaging* **28**, 1023–1036 (2009).
36. K. Gunalan *et al.*, Creating and parameterizing patient-specific deep brain stimulation pathway-activation models using the hyperdirect pathway as an example. *Plos One* **12**, e0176132 (2017).
37. B. Howell *et al.*, Image-based biophysical modeling predicts cortical potentials evoked with subthalamic deep brain stimulation. *Brain Stimul.* **14**, 549–563 (2021).
38. A. M. Noecker *et al.*, StimVision v2: Examples and applications in subthalamic deep brain stimulation for Parkinson's disease. *Neuromodulation* **24**, 248–258 (2021).
39. C. Eliasmith, *How to Build a Brain: A Neural Architecture for Biological Cognition. Reprint edition* (Oxford University Press, 2015).
40. H. Alle, J. R. P. Geiger, Combined analog and action potential coding in hippocampal mossy fibers. *Science* **311**, 1290–1293 (2006).
41. S. Groppa *et al.*, Physiological and anatomical decomposition of subthalamic neurostimulation effects in essential tremor. *Brain* **137**, 109–121 (2014).
42. M. M. Reich *et al.*, Short pulse width widens the therapeutic window of subthalamic neurostimulation. *Ann. Clin. Transl. Neurol.* **2**, 427–432 (2015).
43. M. Åström, E. Diczfalusy, H. Martens, K. Wårdell, Relationship between neural activation and electric field distribution during deep brain stimulation. *IEEE Trans. Biomed. Eng.* **62**, 664–672 (2015).
44. E. H. Middlebrooks, R. A. Domingo, T. Vivas-Buitrago *et al.*, Neuroimaging advances in deep brain stimulation: Review of indications, anatomy, and brain connectomics. *Am. J. Neurodiol.* **41**, 1558–1568 (2020).
45. B. T. T. Yeo *et al.*, The organization of the human cerebral cortex estimated by intrinsic functional connectivity. *J. Neurophysiol.* **106**, 1125–1165 (2011).
46. A. J. Holmes *et al.*, Brain Genomics Superstruct Project initial data release with structural, functional, and behavioral measures. *Sci. Data* **2**, 150031 (2015).
47. P. Mahlknecht *et al.*, Parkinsonian signs in patients with cervical dystonia treated with pallidal deep brain stimulation. *Brain* **141**, 3023–3034 (2018).
48. A. Horn *et al.*, Probabilistic conversion of neurosurgical DBS electrode coordinates into MNI space. *Neuroimage* **150**, 395–404 (2017).
49. R. Nieuwenhuys, J. Voogd, C. van Huijzen, *The Human Central Nervous System* (Springer Science & Business Media, 2013).
50. K. Amunts *et al.*, BigBrain: An ultrahigh-resolution 3D human brain model. *Science* **340**, 1472–1475 (2013).
51. A. Parent, L. De Bellefeuille, Organization of efferent projections from the internal segment of globus pallidus in primate as revealed by fluorescence retrograde labeling method. *Brain Res.* **245**, 201–213 (1982).
52. P. A. Starr *et al.*, Microelectrode-guided implantation of deep brain stimulators into the globus pallidus internus for dystonia: Techniques, electrode locations, and outcomes. *J. Neurosurg.* **104**, 488–501 (2006).
53. W. J. Neumann *et al.*, A localized pallidal physiomarker in cervical dystonia. *Ann. Neurol.* **82**, 912–924 (2017).
54. C. Neudorfer, M. Maarouf, Neuroanatomical background and functional considerations for stereotactic interventions in the H fields of Forel. *Brain Struct. Funct.* **223**, 17–30 (2018).
55. W. Bara-Jimenez, M. J. Catalan, M. Hallett, C. Gerloff, Abnormal somatosensory homunculus in dystonia of the hand. *Ann. Neurol.* **44**, 828–831 (1998).
56. A. Quartarone, H. R. Siebner, J. C. Rothwell, Task-specific hand dystonia: Can too much plasticity be bad for you? *Trends Neurosci.* **29**, 192–199 (2006).
57. Y. Tamura *et al.*, Disordered plasticity in the primary somatosensory cortex in focal hand dystonia. *Brain* **132**, 749–755 (2009).

58. A. Quartarone, A. Pisani, Abnormal plasticity in dystonia: Disruption of synaptic homeostasis. *Neurobiol. Dis.* **42**, 162–170 (2011).
59. A. Conte *et al.*, Primary somatosensory cortical plasticity and tactile temporal discrimination in focal hand dystonia. *Clin. Neurophysiol.* **125**, 537–543 (2014).
60. R. Erro *et al.*, High frequency somatosensory stimulation in dystonia: Evidence fordefective inhibitory plasticity. *Mov. Disord.* **33**, 1902–1909 (2018).
61. D. T. Corp *et al.*, Network localization of cervical dystonia based on causal brain lesions. *Brain* **142**, 1660–1674 (2019).
62. A. Naito, H. Kita, The cortico-pallidal projection in the rat: An anterograde tracing study with biotinylated dextran amine. *Brain Res.* **653**, 251–257 (1994).
63. L. W. Swanson, Cerebral hemisphere regulation of motivated behavior. *Brain Res.* **886**, 113–164 (2000).
64. M. C. Rodríguez-Oroz *et al.*, Initial clinical manifestations of Parkinson's disease: Features and pathophysiological mechanisms. *Lancet Neurol.* **8**, 1128–1139 (2009).
65. J. M. Shine, The thalamus integrates the macrosystems of the brain to facilitate complex, adaptive brain network dynamics. *Prog. Neurobiol.* **199**, 101951 (2021).
66. M. Bologna, A. Berardelli, The cerebellum and dystonia. *Handb. Clin. Neurol.* **155**, 259–272 (2018).
67. M. D. Forrest, M. J. Wall, D. A. Press, J. Feng, The sodium-potassium pump controls the intrinsic firing of the cerebellar Purkinje neuron. *PLoS One* **7**, e51169 (2012).
68. D. P. Calderon, R. Fremont, F. Kraenzlin, K. Khodakhah, The neural substrates of rapid-onset dystonia-Parkinsonism. *Nat. Neurosci.* **14**, 357–365 (2011).
69. P. Filip, O. V. Lungu, M. Bareš, Dystonia and the cerebellum: A new field of interest in movement disorders? *Clin. Neurophysiol.* **124**, 1269–1276 (2013).
70. S. Horisawa, T. Arai, N. Suzuki, T. Kawamata, T. Taira, The striking effects of deep cerebellar stimulation on generalized fixed dystonia: Case report. *J. Neurosurg.* **132**, 712–716 (2019).
71. I. Ilinsky *et al.*, Human motor thalamus reconstructed in 3d from continuous sagittal sections with identified subcortical afferent territories. *eNeuro* **5**, ENEURO.0060-18.2018 (2018).
72. E. G. Jones, The thalamic matrix and thalamocortical synchrony. *Trends Neurosci.* **24**, 595–601 (2001).
73. J. M. Shine, R. Shine, Delegation to automaticity: The driving force for cognitive evolution? *Front. Neurosci.* **8**, 90 (2014).
74. M. E. Larkum, T. Nevian, M. Sandler, A. Polsky, J. Schiller, Synaptic integration in tuft dendrites of layer 5 pyramidal neurons: A new unifying principle. *Science* **325**, 756–760 (2009).
75. T. J. Loher, J. K. Krauss, Dystonia associated with pontomesencephalic lesions. *Mov. Disord.* **24**, 157–167 (2009).
76. R. B. Beck *et al.*, Reduced frequency of ipsilateral express saccades in cervical dystonia: Probing the nigro-tectal pathway. *Tremor Other Hyperkinet. Mov. (N. Y.)* **8**, 592 (2018).
77. H. Karbe, V. A. Holthoff, J. Rudolf, K. Herholz, W. D. Heiss, Positron emission tomography demonstrates frontal cortex and basal ganglia hypometabolism in dystonia. *Neurology* **42**, 1540–1544 (1992).
78. M. Carbon *et al.*, Regional metabolism in primary torsion dystonia: Effects of penetrance and genotype. *Neurology* **62**, 1384–1390 (2004).
79. M. Carbon, M. Argyelan, D. Eidelberg, Functional imaging in hereditary dystonia. *Eur. J. Neurol.* **17** (suppl. 1), 58–64 (2010).
80. C. Gallea *et al.*, Loss of inhibition in sensorimotor networks in focal hand dystonia. *Neuroimage Clin.* **17**, 90–97 (2017).
81. W. J. Neumann *et al.*, Cortico-pallidal oscillatory connectivity in patients with dystonia. *Brain* **138**, 1894–1906 (2015).
82. T. A. Dembek, J. Roediger, A. Horn *et al.*, Probabilistic sweetspots predict motor outcome for DBS in Parkinson's disease. *Ann. Neurol.* **86**, 527–538 (2019).
83. S. A. Eisenstein *et al.*, Functional anatomy of subthalamic nucleus stimulation in Parkinson disease. *Ann. Neurol.* **76**, 279–295 (2014).
84. W. I. A. Haynes, S. N. Haber, The organization of prefrontal-subthalamic inputs in primates provides an anatomical substrate for both functional specificity and integration: Implications for Basal Ganglia models and deep brain stimulation. *J. Neurosci.* **33**, 4804–4814 (2013).
85. M. Li *et al.*, Tractography of the ansa lenticularis in the human brain. *Clin. Anat.***35**, 269–279 (2022).
86. A. Horn *et al.*, Deep brain stimulation induced normalization of the human functional connectome in Parkinson's disease. *Brain* **142**, 3129–3143 (2019).
87. B. Howell, C. C. McIntyre, Analyzing the tradeoff between electrical complexity and accuracy in patient-specific computational models of deep brain stimulation. *J. Neural Eng.* **13**, 036023 (2016).
88. K. Butenko, C. Bahls, M. Schröder, R. Köhling, U. van Rienen, OSS-DBS: Open-source simulation platform for deep brain stimulation with a comprehensive automated modeling. *PLoS Comp. Biol.* **16**, e1008023 (2020).